Neuroscience Research xxx (xxxx) xxx

Contents lists available at ScienceDirect

Neuroscience Research

journal homepage: www.sciencedirect.com/journal/neuroscience-research

Neuronal activity in the anterior paraventricular nucleus of thalamus positively correlated with sweetener consumption in mice

Shaolei Jiang [a,b], Bo Song [a], Zhongdong Liu [c,d], Shuifa Shen [e,f], Weiliang Qian [d], Jing Sun [g], Gaowei Chen [b,*], Yingjie Zhu [b,*]

[a] Key Laboratory of Optical Technology and Instrument for Medicine, Ministry of Education, School of Optical-Electrical and Computer Engineering, University of Shanghai for Science and Technology, Shanghai 200093, China
[b] The Brain Cognition and Brain Diseases Institute of Shenzhen Institute of Advanced Technology, Chinese Academy of Sciences (CAS), Shenzhen 518055, China
[c] Grain College, Henan University of Technology, Zhengzhou 450001, China
[d] Instituto de Física da Universidade de São Paulo, Sã o Paulo 05508-090, Brazil
[e] Hefei Institutes of Physical Science, Chinese Academy of Sciences, Hefei, Anhui 230031, China
[f] School of Intelligent Manufacturing, Zhejiang Guangsha Vocational and Technical University of Construction, Jinhua 322100, China
[g] Department of Anesthesiology, Shenzhen Maternity & Child Healthcare Hospital, The First School of Clinical Medicine, Southern Medical University, No.2004 Hongli Road, Shenzhen 518028, China

ARTICLE INFO

Keywords:
Anterior paraventricular nucleus of the thalamus
Sweeteners
Positive correlation
C-Fos immunohistochemistry
Fiber photometry

ABSTRACT

Although the brain can discriminate between various sweet substances, the underlying neural mechanisms of this complex behavior remain elusive. This study examines the role of the anterior paraventricular nucleus of the thalamus (aPVT) in governing sweet preference in mice. We fed the mice six different diets with equal sweetness for six weeks: control diet (CD), high sucrose diet (HSD), high stevioside diet (HSSD), high xylitol diet (HXD), high glycyrrhizin diet (HGD), and high mogroside diet (HMD). The mice exhibited a marked preference specifically for the HSD and HSSD. Following consumption of these diets, c-Fos expression levels in the aPVT were significantly higher in these two groups compared to the others. Utilizing fiber photometry calcium imaging, we observed rapid activation of aPVT neurons in response to sucrose and stevioside intake, but not to xylitol or water. Our findings suggest that aPVT activity aligns with sweet preference in mice, and notably, stevioside is the sole plant-based sweetener that elicits an aPVT response comparable to that of sucrose.

1. Introduction

The development of sweeteners has undergone a significant evolution since the 19th century (Belloir et al., 2017). Despite the low-calorie properties and cost advantages of artificial sweeteners, human consumption of added sugar remains high (Lim et al., 2010). This observation suggests that many sweeteners may not stimulate the same consumption motivation as refined sugars. Animals show discrimination in their consumption of different sweeteners, influenced by factors such as environmental conditions, energy needs, and perceived reward effects (Begg and Woods, 2013). Yet, the neural mechanisms underpinning these decision-making processes in the central nervous system remain largely unexplored.

Within the central nervous system, the PVT is posited as a critical relay in complex neural circuits that integrate appetite-related information. Specifically, the PVT integrates signals from orexin-expressing hypothalamic energy-sensing neurons and neurons regulating behavioral states, thereby influencing feeding behavior in animals (Kelley and Pratt, 2005). Recent research indicated that the aPVT glutamatergic inputs to the nucleus accumbens (NAc) are instrumental in driving sucrose-seeking behavior (Labouèbe et al., 2016). Zhu et al. (2018) demonstrated that PVT neurons are adept at tracking the context-dependent dynamics of salient information, responding in accordance with the perceived importance of the event. This leads to an intriguing question: Do the responses of PVT neurons mirror the preferences of mice for various sweeteners?

In light of safety concerns associated with artificial synthetic sweeteners (Goran et al., 2018; Mishra et al., 2015), this study focuses on four separate plant-based sweeteners administered to mice. These sweeteners include stevioside (Kujur et al., 2010), xylitol (Borgo et al.,

* Corresponding authors.
E-mail addresses: gw.chen@siat.ac.cn (G. Chen), yj.zhu1@siat.ac.cn (Y. Zhu).

https://doi.org/10.1016/j.neures.2024.02.002
Received 22 August 2023; Received in revised form 2 February 2024; Accepted 7 February 2024
Available online 15 February 2024
0168-0102/© 2024 Published by Elsevier B.V. This is an open access article under the CC BY-NC-ND license (http://creativecommons.org/licenses/by-nc-nd/4.0/).

Table 1
The detailed ingredient list of various sweet feeds.

Product	D10012M		RD18012501		RD18012503		RD18012504		RD18012505		RD18012506	
	AIN-93 M		24% sucrose		25.05% xylitol		0.12% stevioside		0.08% mogroside		0.48% glycyrrhizin	
	10% sucrose											
	gm %	Kcal %	gm %	Kcal %	gm %	Kcal %	gm %	Kcal %	gm %	Kcal %	gm %	Kcal %
Protein	14	*15*	14	*15*	13	*15*	14	*15*	14	*15*	14	*15*
Carbohydrate	73	*76*	73	*76*	75	*76*	73	*76*	73	*76*	73	*76*
Fat	4	*9*	4	*9*	4	*9*	4	*9*	4	*9*	4	*9*
Total		*100*		*100*		*100*		*100*		*100*		*100*
Kcal/gm	3.8		3.8		3.5		3.8		3.8		3.8	
Material	**gm**	***kcal***	**gm**	***kcal***	**gm**	***kcal***	**gm**	***kcal***	**gm**	***kcal***	**gm**	***kcal***
Casein	140	*560*	140	*560*	140	*560*	140	*560*	140	*560*	140	*560*
L- cysteine	1.8	*7.2*	1.8	*7.2*	1.8	*7.2*	1.8	*7.2*	1.8	*7.2*	1.8	*7.2*
Corn starch	495.692	*1982.768*	355.7	*1422.8*	438	*1752*	595.7	*2382.8*	595.7	*2382.8*	595.7	*2382.8*
Maltodextrin	125	*500*	125	*500*	125	*500*	125	*500*	125	*500*	125	*500*
Xylitol	0	*0*	0	*0*	250.5	*631.26*	0	*0*	0	*0*	0	*0*
Stevioside	0	*0*	0	*0*	0	*0*	1.2	*0*	0	*0*	0	*0*
Mogroside	0	*0*	0	*0*	0	*0*	0	*0*	0.8	*0*	0	*0*
Glycyrrhizin	0	*0*	0	*0*	0	*0*	0	*0*	0	*0*	1.2	*0*
Sucrose	100	*400*	240	*960*	0	*0*	0	*0*	0	*0*	0	*0*
Cellulose, BW200	50	*0*	50	*0*	50	*0*	50	*0*	50	*0*	50	*0*
Soybean oil	40	*360*	40	*360*	40	*360*	40	*360*	40	*360*	40	*360*
Tert-butyl hydroquinone	0.008	*0*	0.008	*0*	0.008	*0*	0.008	*0*	0.008	*0*	0.008	*0*
Compound minerals S10022M	35	*0*	35	*0*	35	*0*	35	*0*	35	*0*	35	*0*
Compound vitamin V10037	10	*40*	10	*40*	10	*40*	10	*40*	10	*40*	10	*40*
Choline bitartrate	2.5	*0*	2.5	*0*	2.5	*0*	2.5	*0*	2.5	*0*	2.5	*0*
Lemon yellow	0	*0*	0.05	*0*	0	*0*	0.025	*0*	0.025	*0*	0	*0*
Ttemptation red	0	*0*	0	*0*	0	*0*	0.025	*0*	0	*0*	0	*0*
Edible brilliant blue	0	*0*	0	*0*	0.05	*0*	0	*0*	0.025	*0*	0	*0*
Total	**1000**	***3850***	**1000.058**	***3850***	**1092.858**	***3850***	**1001.258**	***3850***	**1000.858**	***3850***	**1001.208**	***3850***

2021), glycyrrhizin (Somayajulu et al., 2021), and mogroside (Wang et al., 2022). To measure the activity of PVT neurons in mice consuming these sweeteners, we utilized c-Fos immunohistochemical staining and fiber photometry techniques. The results revealed a consistent correlation between the activity of PVT neurons and the sweetener preference behaviors exhibited by the mice.

2. Materials and methods

2.1. Animals

Male C57BL/6 J mice, 8 weeks old, obtained from Charles River Laboratories (Beijing, China), were utilized in these experiments. The mice were housed in an environment with controlled temperature (22–25°C) and humidity (45 ± 5%), and had ad libitum access to food and water, except during experimental sessions. A 12-hour light-dark cycle was rigorously maintained, with lights on from 7:00 am to 7:00 pm. All experimental procedures received approval from the Animal Care and Use Committee of the Shenzhen Institute of Advanced Technology (SIAT), Chinese Academy of Sciences (CAS).

2.2. Solid food intake assays

The high-sweetness diets were prepared and supplied by Shenzhen Ready Biological Medicine Co., Ltd. (Shenzhen, China). Based on the results of molecular simulation or sensory evaluation, we selected the appropriate ratio of sweetness between various sweeteners and sucrose for feed formulation. At 8 weeks of age, 150 mice were randomly assigned to one of 6 groups, with each group containing 25 mice (5 / cage). Data for consumption was shown as the number of cages per group: the HSD group (n = 5) received an HSD containing 9% fat, 15% protein, 76% carbohydrate (kcal), and 24% sucrose; the HSSD group (n = 5) received an HSSD containing 9% fat, 15% protein, 76% carbohydrate (kcal) and 1.2% stevioside (with a sweetness ratio of 1:200 compared to sucrose) (Cardello and Damasio, 1999); HXD group (n = 5) received an HXD containing 9% fat, 15% protein, 76% carbohydrate (kcal) and 25.05% xylitol (with a sweetness ratio of 1:0.9 compared to sucrose) (Park et al., 2017); HGD group (n = 5) received an HGD containing 9% fat, 15% protein, 76% carbohydrate (kcal) and 0.8% glycyrrhizin (with a sweetness ratio of 1:200 compared to sucrose) (Yang et al., 2019); HMD group (n = 5) received an HMD containing 9% fat, 15% protein, 76% carbohydrate (kcal) and 1.2% mogroside (with a sweetness ratio of 1:300 compared to sucrose) (Kasai et al., 1989); The control diet (CD) group (n = 5) was fed a standard laboratory chow diet supplied by Beijing Keao Xieli Feed Co., Ltd. (Beijing, China), consisting of 9% fat, 15% protein, and 76% carbohydrate (kcal). Both the high-sweetness and standard diets were supplemented with essential vitamins and minerals. All diets were formulated to have the same energy density. The detailed composition of these diets is presented in Table 1.

All mice were provided unrestricted access to the control diet. Each mouse cage was equipped with two food boxes, initially both containing standard feed. Following a one-week acclimation period, from 19:00–21:00, one of the boxes in each cage was filled with either CD, HSD, HXD, HSSD, HGD, or HMD, corresponding to the respective groups. The other food box in each cage continued to contain the control diet. At 21:00, the access to the high-sweetness diets was withdrawn for all groups. Subsequently, both food boxes in each cage were refilled with the control diet. The consumption of the CD during the other 22 hours was also recorded. The average food intake and body weight of the mice were calculated based on the mean values for the five mice in each cage. Consequently, the numbers of data for statistical analysis in each group were 5. This procedure lasted for 6 weeks. On the final day, two mice from each cage in the CD, HSD, HXD, and HSSD groups (totaling 10 mice, as there were 5 cages) were randomly selected and anesthetized with pentobarbital sodium 80 mg/kg for immunofluorescence staining at 20:30. Additionally, one mouse from each cage in the CD and HSD groups (5 mice in total) were chosen for light stimulation and then anesthetized with a mixture of ketamine (100 mg/kg) and pelltobarbitalum natricum (60 mg/kg) for c-Fos immunohistochemical staining

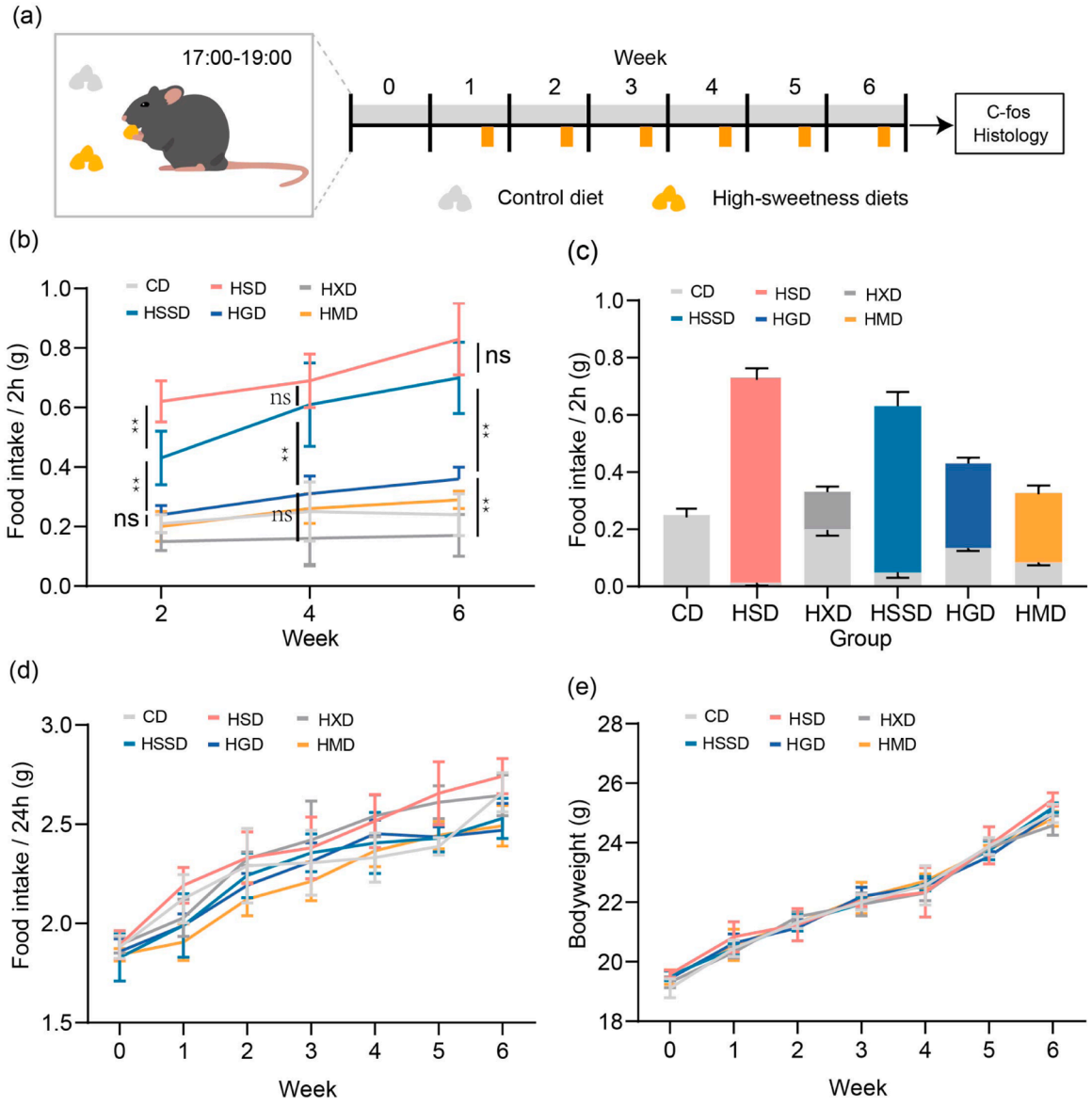

Fig. 1. The consumption of various sweet diets and body weight of mice. (a). The mice underwent intermittent exposure to high-sweetness food for six weeks. (b) Consumption of diets added with different sweeteners from 19:00–21:00 daily for six weeks. The data was presented as an average value of 2 weeks. Cage in CD group, HSD group, HSSD group, HXD group, HGD group, HMD group: n = 5, 5, 5, 5, 5, 5. Two-way ANOVA ($F_{(5, 24)} = 260.8$, $p < 0.0001$), Post-hoc Tukey's test, ** $p < 0.01$, ns, no significant difference. (c) Composition of food intake in each group of mice within 19:00–21:00. The bar graphs of food intake for the other groups of mice, except the CD group, were divided into two parts. The upper was the consumption of a high-sweetness diet, and the lower was the consumption of CD. (d) Mean 24-hour energy intake of mice for six weeks, with the baseline of each group also calculated (Week 0). Two-way ANOVA ($F_{(5, 24)} = 2.227$, $p = 0.0846$), Post-hoc Tukey's test, ns, no significant difference. (e) Body weight changes of mice in each group, with the baseline of each group also calculated (Week 0). Two-way ANOVA ($F_{(5, 24)} = 0.3667$, $p = 0.8708$), Post-hoc Tukey's test, ns, no significant difference. For all graphs, error bars represent the standard error of the mean. See also in Table 2.

(Hristovska et al., 2020; Yang et al., 2022).

In addition, a new batch of 24 mice was randomly allocated into four groups, each comprising six mice. Each mouse was housed in an individual cage. Following the dual feeding box strategy mentioned earlier, from 19:00–21:00, each group of mice was provided with CD, HSD, HXD, or HSSD, respectively. This feeding procedure was conducted over a period of 1 week. On the last day at 20:30, all the mice were anesthetized with a mixture of ketamine (100 mg/kg) and pelltobarbitalum natricum (60 mg/kg) for c-Fos immunohistochemical staining.

To test the differential c-Fos stainability between animals, a LED light controlled by Arduino boards was installed above each cage in a dark environment. This setup provided light flashes at a frequency of 5 Hz for a duration of 30 minutes. The light intensity at the bottom of the cage was maintained at 130 lux (Szatko et al., 2020). One mouse from each of the five cages in both the CD and HSD groups (totaling 5 mice) was selected for light stimulation. Additionally, one mouse from each cage in the CD and HSD groups was kept in a dark environment for at least 90 minutes prior to anesthesia.

2.3. *Liquid food intake assays*

In this study, sweetener solutions of equivalent sweetness were administered to mice during specific experimental phases. Specifically, we prepared solutions of sucrose, xylitol, and stevioside at concentrations of 24%, 25.05%, and 0.12%, respectively, to ensure equivalent sweetness levels. These solutions were created by dissolving the

Table 2
The consumption of different diets by mice in six weeks.

Week	2		4		6	
	Adjusted P Value	Summary	Adjusted P Value	Summary	Adjusted P Value	Summary
CD VS HSD	<0.0001	****	0.0006	***	0.0003	***
CD VS HXD	0.0046	**	0.046	*	0.0462	*
CD VS HSSD	0.0005	***	0.0018	**	0.0019	**
CD VS HGD	0.7822	ns	0.3751	ns	0.0055	**
CD VS HMD	0.9836	ns	0.9916	ns	0.0033	**
HSD VS HXD	<0.0001	****	<0.0001	****	<0.0001	****
HSD VS HSSD	0.0033	**	0.7181	ns	0.3691	ns
HSD VS HGD	<0.0001	****	0.0005	***	0.0043	**
HSD VS HMD	<0.0001	****	0.0003	***	0.0009	***
HXD VS HSSD	<0.0001	****	0.0003	***	0.0005	***
HXD VS HGD	0.0009	***	0.0144	*	0.0007	***
HXD VS HMD	0.0845	ns	0.0563	ns	0.0002	***
HSSD VS HGD	0.0012	**	0.0024	**	0.1077	ns
HSSD VS HMD	0.0005	***	0.0011	**	0.0092	**
HGD VS HMD	0.6456	ns	0.7192	ns	0.1206	ns

predetermined quantities of each sweetener in distilled water.

2.4. C-Fos histology

Mice were deeply anesthetized and transcardially perfused with PBS followed by 4% paraformaldehyde (PFA) in PBS. The brains were removed and postfixed in 4% PFA overnight at 4°C, then cryoprotected in 15% and 30% sucrose solutions until they sank. Coronal brain sections (50 μm) were cut on a cryostat (Leica). For immunostaining, brain sections were rinsed with PBS (3 × 10 min) and then blocked with 10% normal goat serum and 0.3% TritonX-100 in PBS for 2 h at room temperature. Next, sections were incubated with primary antibody (mouse anti-c-Fos, 1:500, Abcam, ab208942, monoclonal) diluted in 5% normal goat serum and 0.3% TritonX-100 in PBS for 24–48 h at 4℃. After washing with PBS (3 × 10 min), sections were incubated with a secondary antibody (Alexa Fluor 488 goat anti-mouse, 1:1000) diluted in 5% normal goat serum and 0.3% Triton X-100 in PBS at room temperature for 2 h and then counterstained with 6-diamidino-2-phenylindole (DAPI).

2.5. Fos distribution and quantification

Fluorescent images were acquired using a slide scanner (Olympus, VS120). The brain slices were aligned and registered to the Allen Mouse Brain Common Coordinate Framework version 3 (CCFv3) (Wang et al., 2020). From each mouse, a brain slice corresponding to the same anteroposterior (AP) axis was obtained. Images with the same brain regions were captured using imaging software (ImageJ). Subsequently, MATLAB (2020b) converted the images into grayscale values, automatically detected the contours of each fluorescent signal, and labeled them. Finally, MATLAB was utilized to automatically count the number of c-Fos positive neurons.

2.6. Surgery

Twenty-eight naive juvenile mice, previously unexposed to sugar, were randomly allocated into four groups CD, HSD, HSSD, and HXD with seven mice per group. Stereotaxic injections were performed on 8-week-old mice anesthetized with pelltobarbitalum natricum (80 mg/kg, i.p.) or a mixture of ketamine (100 mg/kg) and pelltobarbitalum natricum (60 mg/kg), using a stereotaxic device (BenchMARK Digital, Lecia). A glass capillary, pulled to a fine point and attached to a Micro 4 pressure nanoinjector (World Precision Instruments), delivered 200 nl of AAV virus solution into the aPVT (coordinates: bregma −1.2 mm, lateral 0.15 mm, ventral 3.0 mm, with a 5° angle toward the midline) at a rate of 60 nl/min. After completing the injection, the needle was left in place for an additional 5 minutes to ensure proper diffusion of the solution. Subsequently, a plastic fiber-optic cannula (OD., 200 μm , NA = 0.37) was inserted 200–400 μm above the injection site and secured to the skull using dental cement (Lang Dental Manufacturing). The mice were allowed a recovery period of at least three weeks for virus expression before commencing behavioral training. The adeno-associated viruses (AAVs) utilized in this study were sourced from Shanghai Taitool Bioscience Co., Ltd.

2.7. Fiber photometry

Three weeks post-infection with the AAV virus, the mice commenced behavioral training. All the mice were provided with a CD. The mice were placed in a behavioral box equipped with a hole in one wall, into which a metal tube was inserted. Mice underwent water deprivation for 24 hours prior to the training session. When they entered the box, they naturally explored the hole and bit the metal tube. When their tongue contacted the tip of the tube, a sweet solution was delivered. Subsequently, mice in the CD, HSD, HXD, and HSSD groups were provided with water, sucrose solution, and stevioside solution, respectively. After three days of continuous training, mice learned to obtain fluid by licking the tip of the tube, and water was restored after each session. Behavioral tests were subsequently conducted, allowing mice to freely move and lick the tube without restriction, with the system recording the timing of each lick. Following multiple training sessions, freely moving mice received 6 μl of liquid each time they licked the tip of the metal tube. The first lick by the mouse triggers the start of a trial, during which the mouse can lick the metal spout unlimitedly. The trial will end when there is no further lick action within 6 seconds. And the subsequent licks immediately trigger new trials. The number of licking actions of the mouse in each trial will be calculated. Calcium signals within the time window of 6 s before and 8 s after the start of each trial will be segmented and extracted for analysis (Chen et al., 2022). Calcium signals were measured using a fiber photometry system (Thinker Tech Nanjing Biotech Co., Ltd, China). Calcium-dependent fluorescence signals were obtained by stimulating cells expressing GCaMP6s with a 470 nm laser (40 μW at fiber tip). Photometry data were normalized (Z-score) using MATLAB. We extracted and plotted the calcium signal data for each trial. Baseline normalization was performed on the original ΔF/F signals. Thus, Z-scores accurately reflect the number of standard deviations from the mean, and the baseline may not be at zero. The area under the curve (AUC) was employed as a measure of neuronal activity (Yoshida et al., 2023). The AUC within the −1 s to 2 s following time windows of the first lick action in each trial is extracted for inter-group comparisons in mice.

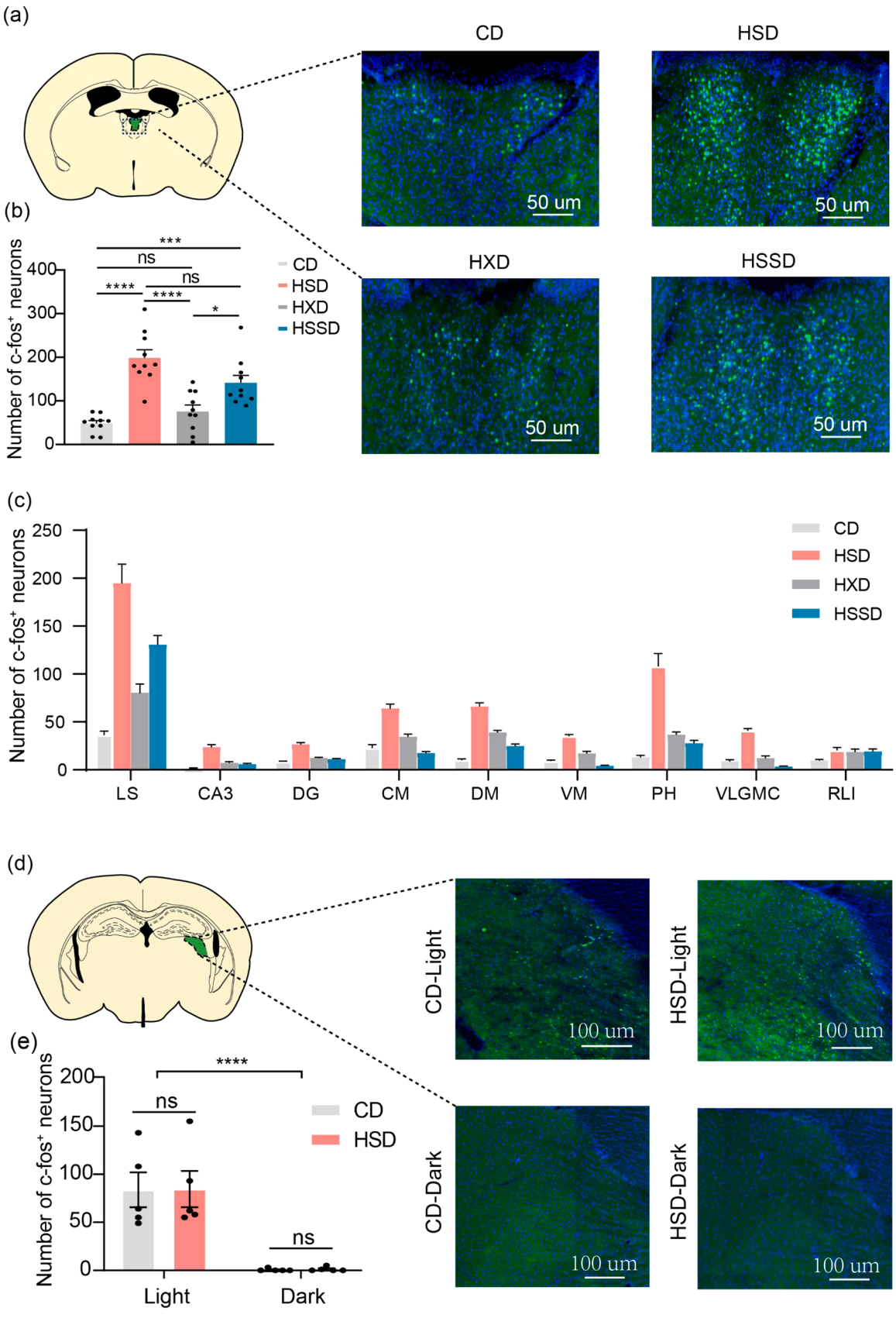

(caption on next page)

Fig. 2. The c-Fos expression of the brain in mice exposed to an intermittent high-sweetness diet for 6 weeks. (a) C-Fos immunoreactivity results of aPVT of mice in each group. (b) Number of c-Fos positive neurons in aPVT of mice in each group, symbols reflect individual subject values and error bars reflect the standard error of the mean. Mice in CD group, HSD group, HXD group, HSSD group: n = 10,10,10,10; One-way ANOVA ($F_{(3,36)} = 20.09$, $p < 0.0001$), Post-hoc Tukey's test, * $p < 0.05$, ** $p < 0.01$, *** $p < 0.001$, **** $p < 0.0001$, ns, no significant difference]. (c) Number of c-Fos positive neurons in lateral septum (LS), One-way ANOVA ($F_{(3,36)} = 30.12$, $p < 0.0001$); hippocampal CA3 (CA3), One-way ANOVA ($F_{(3,36)} = 39.41$, $p < 0.0001$); dentate gyrus (DG), One-way ANOVA ($F_{(3,36)} = 40.18$, $p < 0.0001$); central medial nucleus of the thalamus (CM), One-way ANOVA ($F_{(3,36)} = 35.93$, $p < 0.0001$); dosomedial nucleu of the hypothalamus (DM), One-way ANOVA ($F_{(3,36)} = 82.77$, $p < 0.0001$); ventral medial nucleus of hypothalamus (VM), One-way ANOVA ($F_{(3,36)} = 79.98$, $p < 0.0001$) posterior hypothalamus (PH), One-way ANOVA ($F_{(3,36)} = 35.37$, $p < 0.0001$); ventral lateral geniculate nucleus, magnocellular part (VLGMC), One-way ANOVA ($F_{(3,36)} = 75.43$, $p < 0.0001$); and rostral linear nucleus of raphe (RLI), One-way ANOVA ($F_{(3,36)} = 3.518$, $p = 0.0246$). Post-hoc Tukey's test, * $p < 0.05$, ** $p < 0.01$, *** $p < 0.001$, **** $p < 0.0001$, ns, no significant difference. (d) The expression of c-Fos in the LGN of mice is induced by light stimulation. (e) Number of c-Fos positive neurons in LGN [CD group (n = 5) VS HSD group (n = 5). Light stimulation factors: Two-way ANOVA ($F_{(1,16)} = 40.61$, $p < 0.0001$). Diet factors: Two-way ANOVA ($F_{(1,16)} = 0.0029$, $p = 0.9580$)]. See also in Table 3.

2.8. Statistical analysis

Statistical analysis was performed using GraphPad Prism 8.0. Two-way ANOVA followed by the post hoc Tukey's test was used to compare more than two experimental groups with time variables. One-way ANOVA followed by post hoc Tukey's test was used to compare more than two experimental groups without time variables. Data are presented as means ± s.e.m. Statistical significance levels are indicated as follows: * $p < 0.05$, *** $p < 0.001$, **** $p < 0.0001$.

3. Results

3.1. Preference patterns in mice exposed to various high-sweetness diets

Following six weeks of intermittent exposure to high-sweetness feed, the mice developed a stable preference phenotype (Fig. 1a). Mice exhibited a preference for HSD and HSSD (Fig. 1b). During the 19:00–21:00 feeding period, their consumption averaged 0.62 ± 0.07 g for HSD and 0.43 ± 0.09 g for HSSD, significantly exceeding that of the CD group. However, the intake of HSSD was lower compared to HSD. In contrast, mice did not prefer HXD, HGD, and HMD, consuming 0.12 ± 0.03 g HXD, and 0.2 ± 0.09 g HMD respectively in this period, which was even lower than that of the CD group. The consumption of HMD was similar to that of CD. After four weeks, the preference for HSSD significantly increased, while interest in HXD and HMD remained negligible. The consumption of HGD by mice increased, but it was still significantly lower than that of HSSD. The detailed statistical results are presented in Table 2.

In addition to the high-sweetness diet, mice also consumed varying amounts of the CD during this period. During the 19:00–21:00 feeding window, the mice consumed predominantly of HSD and HSSD, accounting for 97% and 92%, in these two groups. In the HGD and HMD groups, mice consumed 69% and 75% of their diet as the sweetened diet, respectively (Fig. 1c).

Overeating and being overweight due to the palatability of high-sweetness foods is a sensitive issue related to sugar consumption. Therefore, we calculated the average total daily energy intake throughout the experiment (Fig. 1d), and also monitored the weight changes in each mouse group (Fig. 1e). The data showed that the average 24-hour energy intake of mice in each group was similar. While mice on a high sucrose diet acutely consumed substantial amounts of HSD, they compensated by reducing their CD intake at other times, thereby maintaining a balance in total energy intake and avoiding overweight, consistent with previous reports (Mungarndee and Norgren, 2008).

These data indicate that the preference of mice for sucrose, stevioside, and xylitol differed significantly at the concentration we used, while the preference for glycyrrhizin and mogroside was intermediate between the two groups (stevioside and xylitol).

3.2. C-Fos expression in aPVT linked to sweetener preferences

We next performed immunostaining for c-Fos, a marker of recent neuronal activity, to examine the feeding-activated neurons across the entire brain. Given the notable differences in preference for stevioside and xylitol, we focused on these two groups, along with the HSD group. We observed c-Fos immunofluorescent signals in numerous brain regions. Among them, the abundance of fluorescence signals in the aPVT showed potential consistency with the mice's food consumption. Initially, we observed significant differences in c-Fos expression levels within the aPVT among the various groups (Fig. 2a). The HSD group had 198.5 ± 18.77c-Fos$^+$ neurons in aPVT, which was significantly higher than the CD and HXD groups. the HSSD group exhibited 141.4 ± 17.19c-Fos$^+$ neurons, a count comparable to the HSD group and significantly greater than both the CD and HXD groups (Fig. 2b). Mice in the HXD group demonstrated a level of c-Fos expression similar to that of the control group. There were also c-Fos$^+$ neurons in other brain regions (Fig. 2c), such as lateral septum (LS), hippocampal CA3, and dorsomedial Hypothalamic Nucleus (DM), ventromedial hypothalamus (VM), and posterior hypothalamus (PH). This observation indicates that the consumption of different sweeteners led to varying degrees of neuronal activation in these brain regions across the different groups. The statistical results are presented in Table 3. Additionally, we verified the stainability of c-Fos across different animals. Upon comparing c-Fos expression levels in the lateral geniculate body (LGN), a crucial brain structure for processing visual information (Hooks and Chen, 2020; Mirochnik and Pezaris, 2019), no significant difference was observed between the CD and HSD group mice after exposure to identical light stimulation (Fig. 2d, e).

During the final stage of intermittent exposure to high-sweetness diets, mice exhibited no significant difference in consumption of HSSD and HSD. And there was no significant difference in c-Fos expression in the aPVT between these two groups. Initially, HSD was significantly more attractive to the mice, as evidenced by their notably higher consumption of HSD compared to the HSSD group (Fig. 1b). To establish a more precise correlation between aPVT activity and the mice's food preferences, a new batch of mice was subjected to a brief 1-week high-sweetness diet exposure, followed by c-Fos immunohistochemical staining on the final day. Over the 1-week period of intermittent high-sweetness diet exposure (Fig. 3a), mice consumed 0.62 ± 0.05 g HSD (Fig. 3b), which was significantly more than the HSSD group. Furthermore, the number of c-Fos positive neurons in the aPVT of the HSD group was significantly surpassing that in the HSSD group (Fig. 3c, d). The c-Fos expression in the aPVT of the HSSD group was also higher than the CD and HXD group. One week exposure to various sweet diets led to a consistent pattern of c-Fos expression in the aPVT, corresponding with their respective food intake levels.

3.3. aPVT neurons activity responding to different sweeteners

We then proceeded to examine the real-time responses of aPVT neurons to various sweeteners consumed by the mice, using fiber photometry calcium imaging methods. For this purpose, mice expressing the GCaMP6s calcium indicator in the aPVT were selected for in vivo calcium imaging. (Fig. 4a, b). Upon presentation of sucrose solutions, mice performed 88.9 ± 13.2 licks (Fig. 4c), resulting in the consumption

Table 3
C-Fos positive neurons in the whole brain.

LS	Mean 1	Mean 2	sig	p value
CD VS HSD	36.1±4.27	194.7±19.91	****	<0.0001
CD VS HXD	36.1±4.27	82.3±9.95	ns	<0.0562
CD VS HSSD	36.1±4.27	130.5±9.89	****	<0.0001
HSD VS HXD	194.7±19.91	82.3±9.95	****	<0.0001
HSD VS HSSD	194.7±19.91	130.5±9.89	**	<0.0041
HXD VS HSSD	82.3±9.95	130.5±9.89	*	0.0432
DG	**Mean 1**	**Mean 2**	**sig**	**p value**
CD VS HSD	8.4±0.76	26.4±2.10	****	<0.0001
CD VS HXD	8.4±0.76	12.2±0.9	ns	0.1708
CD VS HSSD	8.4±0.76	11±0.83	ns	0.4832
HSD VS HXD	26.4±2.10	12.2±0.9	****	<0.0001
HSD VS HSSD	26.4±2.10	11±0.83	****	<0.0001
HXD VS HSSD	12.2±0.9	11±0.83	ns	0.9096
DM	**Mean 1**	**Mean 2**	**sig**	**p value**
CD VS HSD	10.1±1.25	66±3.90	****	<0.0001
CD VS HXD	10.1±1.25	38.9±2.31	****	<0.0001
CD VS HSSD	10.1±1.25	24.7±2.31	**	0.0019
HSD VS HXD	66±3.90	38.9±2.31	****	<0.0001
HSD VS HSSD	66±3.90	24.7±2.31	****	<0.0001
HXD VS HSSD	38.9±2.31	24.7±2.31	**	0.0026
PH	**Mean 1**	**Mean 2**	**sig**	**p value**
CD VS HSD	12.8±2.2	107.9±13.37	****	<0.0001
CD VS HXD	12.8±2.2	36.6±2.94	ns	0.102
CD VS HSSD	12.8±2.2	27.5±3.13	ns	0.4704
HSD VS HXD	107.9±13.37	36.6±2.94	****	<0.0001
HSD VS HSSD	107.9±13.37	27.5±3.13	****	<0.0001
HXD VS HSSD	36.6±2.94	27.5±3.13	ns	0.8023
RLI	**Mean 1**	**Mean 2**	**sig**	**p value**
CD VS HSD	9.6±1.44	20.4±2.84	*	0.0297
CD VS HXD	9.6±1.44	18.5±3.16	ns	0.095
CD VS HSSD	9.6±1.44	19±2.72	ns	0.0712
HSD VS HXD	20.4±2.84	18.5±3.16	ns	0.9556
HSD VS HSSD	20.4±2.84	19±2.72	ns	0.9814
HXD VS HSSD	18.5±3.16	19±2.72	ns	0.9991
CA3	**Mean 1**	**Mean 2**	**sig**	**p value**
CD VS HSD	1.4±0.45	23.5±2.64	****	<0.0001
CD VS HXD	1.4±0.45	7.2±1.13	ns	0.0541
CD VS HSSD	1.4±0.45	5.7±1.02	ns	0.2177
HSD VS HXD	23.5±2.64	7.2±1.13	****	<0.0001
HSD VS HSSD	23.5±2.64	5.7±1.02	****	<0.0001
HXD VS HSSD	7.2±1.13	5.7±1.02	ns	0.9012
CM	**Mean 1**	**Mean 2**	**sig**	**p value**
CD VS HSD	22.7±3.51	63.9±4.85	****	<0.0001
CD VS HXD	22.7±3.51	34.2±3.07	ns	0.1074
CD VS HSSD	22.7±3.51	17.3±1.74	ns	0.692
HSD VS HXD	63.9±4.85	34.2±3.07	****	<0.0001
HSD VS HSSD	63.9±4.85	17.3±1.74	****	<0.0001
HXD VS HSSD	34.2±3.07	17.3±1.74	**	0.0077
VM	**Mean 1**	**Mean 2**	**sig**	**p value**
CD VS HSD	9±1.01	35.2±1.60	****	<0.0001
CD VS HXD	9±1.01	17±2.23	**	0.0039
CD VS HSSD	9±1.01	4±0.91	ns	0.1147
HSD VS HXD	35.2±1.60	17±2.23	****	<0.0001
HSD VS HSSD	35.2±1.60	4±0.91	****	<0.0001
HXD VS HSSD	17±2.23	4±0.91	****	<0.0001
VLGMC	**Mean 1**	**Mean 2**	**sig**	**p value**
CD VS HSD	8.7±1.76	40.7±2.24	****	<0.0001
CD VS HXD	8.7±1.76	11.9±2.50	ns	0.6483
CD VS HSSD	8.7±1.76	3.2±0.76	ns	0.2019
HSD VS HXD	40.7±2.24	11.9±2.50	****	<0.0001
HSD VS HSSD	40.7±2.24	3.2±0.76	****	<0.0001
HXD VS HSSD	11.9±2.50	3.2±0.76	*	0.0151

of 533.1 ± 79.3 μl of sucrose solution (Fig. 4d). Conversely, the mice consumed 184.3 ± 36.1 μl of water, 526.3 ± 114.3 μl of stevioside solution (87.7 ± 19.0 licks), and 163.7 ± 50.9 μl of xylitol solution (27.3 ± 8.5 licks), respectively. The consumption of sucrose and stevioside was significantly greater than that of the other liquids. There was no significant difference in the frequency of licking actions per trial among mice in these groups (Fig. 4e).

In the HSD and HSSD groups, calcium signals in the aPVT began to rapidly increase prior to the consumption of the liquid, peaking at the moment the sweetener was tasted, and subsequently declined (Fig. 4f). Conversely, calcium signals in the aPVT of mice in the CD and HXD groups did not exhibit significant fluctuations during this behavior. The area under the curve (AUC) of the calcium signals revealed that the aPVT activity in mice of the HSSD group while licking stevioside was comparable to that in the HSD group (Fig. 4g), and significantly higher than that observed in the CD and HXD groups.

4. Discussion

Sweet-tasting foods, particularly those with added sugars, have been shown to stimulate human appetite (Venditti et al., 2020). Previously, many researchers have investigated the neural mechanism of sweetness preference behavior (Frank et al., 2008). Magnetic resonance imaging (MRI) studies have revealed that sucrose intake induces significantly more global brain activation than the artificial sweetener saccharin, including in regions such as the insula, thalamus, and substantia nigra (Haase and Murphy, 2008). (Tellez et al., 2016) also reported that dopamine release in the dorsal striatum increased above baseline only when sucralose intake was paired with intragastric infusions of glucose, but not when sucralose was consumed alone. Contrastingly, certain brain nuclei, such as the right amygdala, exhibited greater activation with non-caloric beverages compared to caloric ones prior to consumption (Smeets et al., 2011). Additionally, the activity in well-known central taste relays, including the nucleus of the solitary tract (NTS) and the parabrachial nucleus (PBN), has been extensively studied in relation to visceral nutritional signals. (Loney and Eckel, 2021) found that ingestion of the non-caloric sweetener sucralose solution also activated c-Fos expression in the NTS. Mungarndee, Norgren, (Mungarndee and Norgren, 2008) showed that sham ingestion of sucrose, i.e., ingested sucrose was drained through a gastric fistula, also induced high c-Fos expression in the PBN. Taken together, this collection of findings suggests that the central nervous system differentiates between sucrose and other sweeteners by eliciting distinct responses. These variations in neural activation across different brain regions highlight the complexity of how the brain perceives and processes the sweetness of various substances.

Measuring animal preferences and correlating them with real-time brain responses seems to be a reliable approach, as evidenced by the results of this study. In our experiments, we provided mice with sweet diets of equal energy density thereby minimizing the impact of visceral sensory stimulation on central nervous feedback signals, which could influence aPVT neuron activity (Rogers and Blundell, 1989). Of course, in the initial stages of encountering high-sweetness diet, mice did indeed show a stronger preference for sucrose feed, which perhaps could be driven by the unique nutritional signals from sucrose. Notably, among the liquid foods offered, only the sucrose solution had significant caloric content. Given that nutrient constituents transmit feedback signals to the central nervous system, which in turn regulate feeding behavior through visceral organs (Tellez et al., 2016), we anticipated specific aPVT neuron responses when mice licked the sucrose solution. Contrary to expectations, our results demonstrated similar real-time aPVT neuron responses to both stevioside and sucrose solutions. Nevertheless, we observed subtle differences between the mice in the HSD and HSSD groups. After licking the sucrose solution, the calcium signals remained stably elevated, while mice licking the stevioside solution showed a return of calcium signals to baseline levels with mild periodic fluctuations similar to the baseline. These observed differences might be attributed to variations in the nutritional values of the sweeteners. This suggests that aPVT neurons may inevitably engage in the perception of nutritional signals. However, when licking different sweet liquids, nutritional value is not the sole factor provoking a robust response in the aPVT. However, the current study does not fully elucidate the visceral stimulation effects caused by the six sweeteners, nor does it explore how visceral signals might interfere with PVT responses. This gap in understanding presents a direction for our future research. Finally, our findings corroborate previous observations by (Mungarndee and Norgren,

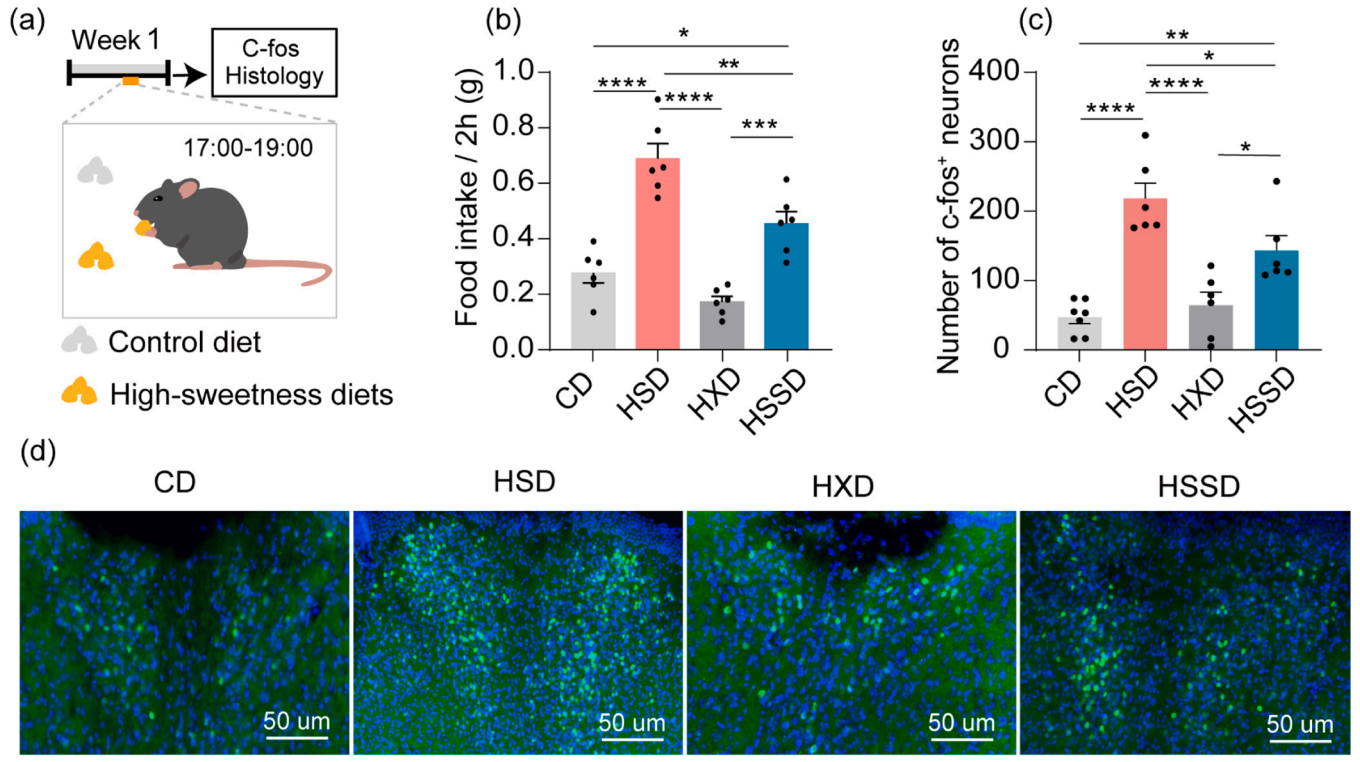

Fig. 3. he c-Fos expression of the brain in mice exposed to an intermittent high-sweetness diet for 1 week. (a) The mice underwent intermittent exposure to high-sweetness food for one week. (b) Consumption of diets added with different sweeteners from 19:00–21:00 daily for 1 week. (c) Number of c-Fos positive neurons in aPVT of mice in each group; symbols reflect individual subject values, and error bars reflect the standard error of the mean. (d) C-Fos immunoreactivity results of aPVT of mice in each group. Mice in CD group, HSD group, HSSD group, HXD group: n = 10, 10, 10, 10; One-way ANOVA ($F_{(3,36)} = 20.09$, $p < 0.0001$), Post-hoc Tukey's test, * $p < 0.05$, ** $p < 0.01$, *** $p < 0.001$, **** $p < 0.0001$, ns, no significant difference.

2008), indicating that although mice exhibited significant overeating when exposed to HSD and HSSD, they compensated by reducing their intake of regular food at other times, thereby avoiding overweight.

In this study, our focus was exclusively on the correlation between aPVT neuron activity and sweetener consumption in male animals. However, it is crucial to acknowledge that behavioral differences between male and female animals do exist in hedonic feeding models. Notably, female animals have been observed to be more prone to binge-eating symptoms. This sex-specific disparity underscores the importance of considering sex differences in future research to obtain a more comprehensive understanding of hedonic feeding behaviors and the underlying neural mechanisms (Mitchell and Shaw, 2015). (Parsons et al., 2022) reported a notable finding where postprandial female rats exhibited a significant increase in fos expression in the posterior paraventricular thalamus (pPVT) after consuming high-sugar solid food, a response that was not as pronounced in male rats. This observation suggests potential differences in aPVT responses between male and female rodents when consuming various sweetened feeds. Such sex-based differences in neural response patterns underscore the necessity for further experimental validation to better understand these variations and their implications in the broader context of nutritional neuroscience. Contrasting with Parsons' experimental setup, our study involved mice entering the dark phase of their light-dark cycle at 19:00. This timing could introduce varying degrees of appetite among the mice due to potential awakening mechanisms. Such circadian influences are critical to consider, as they may significantly affect feeding behavior and neural responses. This aspect of our experimental design highlights the complexity of studying animal behavior and the necessity of accounting for environmental factors like the light-dark cycle, which could modulate the animals' natural behaviors and responses (Chen et al., 2022). This may explain the presence of c-Fos expression in aPVT across all mice.

The aPVT is known to play a significant role in regulating food-seeking behavior (Cheng et al., 2022). It receives orexigenic signals from the hypothalamus, participating in the regulation of sleep-wake cycles and maintaining heightened neuronal excitability during wakefulness (Ren et al., 2018). Furthermore, this pathway is implicated in energy sensing and behavioral state regulation, transmitting signals to cholinergic interneurons in the downstream striatum, thereby extending feeding-related motivational states beyond immediate energy needs (Kelley and Pratt, 2005). Consistently, the activation of orexin receptors in the PVT implicates its involvement in regulating hedonic feeding behavior (Choi et al., 2012). Additionally, the PVT receives dense γ-aminobutyric acid (GABA) projections from the zona incerta (ZI), which play a crucial role in the regulation of feeding behavior (Zhang and van den Pol, 2017). In addition to internal signals related to energy balance, the aPVT also integrates prominent visceral sensory information, including gustatory inputs, to modulate appetite (Millan et al., 2017). The aPVT exerts its functions by connecting to downstream brain regions through multiple pathways, Christoffel, et al. (Christoffel et al., 2021) demonstrated that the aPVT→NAc projection plays a pivotal role in reward-seeking behavior, acting as an interface for reward processing by integrating various inputs. And the repeated exposure to palatable food leads to specific strengthening of synaptic connections within this neural circuit (Christoffel et al., 2021). Consequently, after six weeks of providing mice with high-sweetness food, it is plausible that neurons in the PVT may undergo synaptic plasticity changes, an area warranting further research. During intermittent exposure to high-sweetness diets, mice display increased consumption of both HSD and HSSD, accompanied by elevated c-Fos expression in the aPVT. This process involves energy balance, reward effects, learning, and memory, with the PVT effectively integrating these signals to make feeding decisions (Petrovich, 2018). Cheng, et al. (Cheng et al., 2022) also reported that the intake of high-fat food induced heightened c-Fos expression in the aPVT.

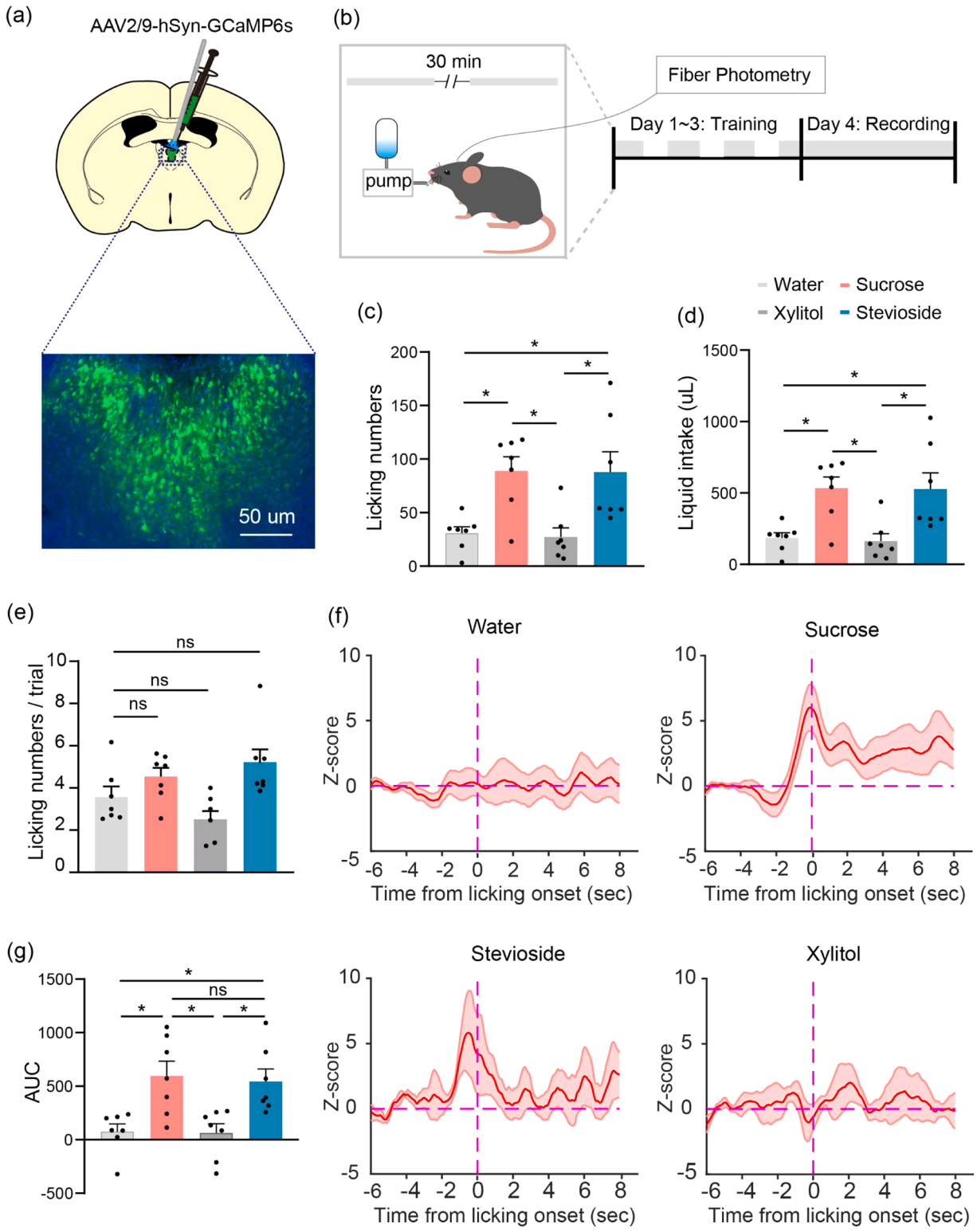

Fig. 4. The calcium signals of neurons in aPVT. (a)Viral targeting of AAV2/9-hSyn-GCaMP6s-WPRE-pA into the aPVT, the tip of fiber optic above the aPVT, and the viral expression of GCaMP6s in aPVT. (b) The training paradigm for mice involves freely moving subjects that lick metal tubes to obtain corresponding sweet liquids. The behavioral testing lasts for 30 minutes. (c) The licking numbers of the corresponding sweet liquid in each group of mice within 30 minutes mice in CD group, HSD group, HSSD group, HXD group: n = 7,7,7,7; One-way ANOVA ($F_{(3,24)} = 7.436$, $p = 0.0011$), Post-hoc Tukey's test, * $p < 0.05$, ** $p < 0.01$, ns, no significant difference. (d) Intake of corresponding sweet liquid for mice in each group, One-way ANOVA ($F_{(3,24)} = 7.277$, $p = 0.0012$). (e) Licking numbers per trial of the mice when they consumed the corresponding sweet liquid, One-way ANOVA ($F_{(3,24)} = 5.378$, $p = 0.0056$). (f) Calcium signals of aPVT neurons when mice in each group consumed the corresponding sweet liquid. (g) The AUC of calcium signals in aPVT when mice in each group consumed the corresponding sweet liquid, One-way ANOVA ($F_{(3,24)} = 7.277$, $p = 0.0012$. Post-hoc Tukey's test, * $p < 0.05$, ** $p < 0.01$, ns, no significant difference. For all graphs, symbols reflect individual subject values and error bars reflect the standard error of the mean. AUC, the area under the curve (see methods). For all graphs, symbols reflect individual subject values and error bars reflect the standard error of the mean.

We also observed notable c-Fos expression in the LS. Given the LS's involvement in feeding behavior and reward processing (Chen et al., 2022; Sternson and Eiselt, 2017), the activity within this nucleus likely plays a significant role in animals' preference for sweeteners within the broader neural circuit. Additionally, in other brain regions like the DM (Knight et al., 2017), VM (Chao et al., 2011), and PH (Inada et al., 2022), we found that c-Fos expression induced by sucrose intake was significantly higher compared to other sweeteners. These regions are closely related to the energy homeostasis regulation of the animal body. Compared with other sweet feeds whose carbohydrate sources are almost entirely starch, sucrose in HSD can directly provide energy. More importantly, compared with starch, intake of equal or even less caloric value of sucrose can increase blood glucose to a greater extent and maintain a sustained relatively high blood glucose level (Kienzle, 1994; Koytchev, et al., 2009). Under the conditions of nutrient-rich and energy storage excess, these hypothalamic regions will be activated to regulate energy intake and reduce nutrient availability (reduce endogenous glucose production) (Morton, 2007). This observation suggests a series of energy homeostasis signals potentially triggered by the mice's more pronounced consumption response to HSD.

The correlation between the real-time activity of neurons in the brain and the preference of animals for sweeteners has also been examined. (Otis et al., 2019) demonstrated that during the early stages of cue-paired reward-seeking behavior training, head-fixed mice passively receiving a sucrose solution exhibited a rise in calcium signals within the PVT only after initiating licking. After multiple training sessions, the calcium signals in PVT would begin to rise sharply as soon as cues were presented, peak at the instant of licking, and then return to baseline levels. In our experiment, we observed an upward trajectory in calcium signals even before the mice licked the metal spout, a response often indicative of reward anticipation in mice (Choi and McNally, 2017; Hsu et al., 2014), and the rewarding value is largely provided by the palatable flavors of sucrose solution and stevioside solution. Therefore, the PVT region may integrate multiple sources of information, such as taste, hedonic value, and nutritional value, and ultimately participate in decision-making. To accurately assess potential differences in calcium signaling of PVT neurons during these periods, this study meticulously controlled the licking behavior across different groups of mice, ensuring uniformity in the number and frequency of licks. This approach further contributes to elucidating the relationship between PVT response in mice and their preference for sucrose and stevioside.

In summary, our study demonstrates that the aPVT neurons are selectively activated by preferred sweeteners, namely sucrose and stevioside, but not by less preferred options. Furthermore, we observed a positive correlation between the activity of these neurons and the intake of sweeteners by mice. These findings shed light on the neural underpinnings of sweet taste preferences in animals and offer valuable insights for the development of new sweetener products.

CRediT authorship contribution statement

Shen Shuifa: Methodology. **Liu Zhongdong:** Methodology. **Song Bo:** Methodology. **Jiang Shaolei:** Data curation, Formal analysis, Investigation, Methodology, Software, Writing – original draft. **Chen Gaowei:** Conceptualization, Data curation, Methodology, Writing – review & editing. **Sun Jing:** Formal analysis, Funding acquisition. **Zhu Yingjie:** Funding acquisition, Project administration, Supervision, Validation, Writing – review & editing. **Qian Weiliang:** Methodology.

Acknowledgments

This work was supported by the National Natural Science Foundation of China (81922024), the Science, Technology, and Innovation Commission of Shenzhen Municipality (RCJC20200714114556103, ZDSYS20190902093601675 and JCYJ20190809170605515), Shenzhen Maternity & Child Healthcare Hospital Science Foundation (FYA2022003).

Author contributions

In this work, Z. L. and Y. Z. conceived the study. S. J. and G. C. recorded the food consumption and body weight of the mice. S. J. and G. C. and S. J. performed immunohistochemical staining, and S. J. performed virus injection experiments and fiber photometry recording. B. S., S. S., W. Q., and S. J. provided the maintenance of experimental equipment and the methods of data analysis. S. J. performed data analysis. All the authors approved the present submitted version.

Disclosure statement

The authors declare no competing financial interests.

References

Begg, D.P., Woods, S.C., 2013. The endocrinology of food intake. Nat. Rev. Endocrinol. 9 (10), 584–597.
Belloir, C., Neiers, F., Briand, L., 2017. Sweeteners and sweetness enhancers. Curr. Opin. Clin. Nutr. Metab. Care 20 (4), 279–285.
Borgo, J., Laurella, L., Martini, M.F., Catalan, C., Sulsen, V., 2021. Stevia Genus: Phytochemistry and Biological Activities Update. Molecules 26 (9), 2733.
Cardello, H.M., Damasio, M.H., 1999. Measurement of the relative sweetness of stevia extract, aspartame and cyclamate/saccharin blend as compared to sucrose at different concentrations. Plant Foods Hum. Nutr. 54 (2), 119–130.
Chao, P.T., Yang, L., Aja, S., Moran, T., Bi, S., 2011. Knockdown of NPY expression in the dorsomedial hypothalamus promotes development of brown adipocytes and prevents diet-induced obesity. Cell Metab. 13 (5), 573–583.
Chen, Z., Chen, G., Zhong, J., Lai, S., Xu, H., Deng, X., Li, F., Lu, S., Zhou, K., Li, C., Liu, Z., Zhang, X., Zhu, Y., 2022. A circuit from lateral septum neurotensin neurons to tuberal nucleus controls hedonic feeding. Mol. Psychiatry 27 (12), 4843–4860.
Cheng, J., Ma, X., Li, C., Ullah, R., Wang, X., Long, J., Yuan, Z., Liu, S., Fu, J., Chen, Z., Shen, Y., Zhou, Y.D., 2022. Diet-induced inflammation in the anterior paraventricular thalamus induces compulsive sucrose-seeking. Nat. Neurosci. 25 (8), 1009–1013.
Choi, D.L., Magrisso, I.J., Fitzgerald, M.E., Lipton, J.W., Benoit, S.C., 2012. Orexin signaling in the paraventricular thalamic nucleus modulates mesolimbic dopamine and hedonic feeding in the rat. Neuroscience 17 (210), 1873–7544.
Choi, E.A., McNally, G.P., 2017. Paraventricular Thalamus balances danger and reward. J. Neurosci. 37 (11), 3018–3029.
Christoffel, D.J., Walsh, J.J., Heifets, B.D., Hoerbelt, P., Neuner, S., Sun, G., Ravikumar, V.K., Wu, H., Halpern, C.H., Malenka, R.C., 2021. Input-specific modulation of murine nucleus accumbens differentially regulates hedonic feeding. Nat. Commun. 12 (1), 2135.
Frank, G., Oberndorfer, T., Simmons, A., Paulus, M., Fudge, J., Yang, T., Kaye, W., 2008. Sucrose activates human taste pathways differently from artificial sweetener. NeuroImage 39 (4), 1559–1569.
Goran, M., Plows, J., Ventura, E., 2018. Effects of consuming sugars and alternative sweeteners during pregnancy on maternal and child health: evidence for a secondhand sugar effect. Proc. Nutr. Soc. 78 (3), 1–10.
Haase, L., Murphy, C., 2008. Cortical activation in response to pure taste stimuli during the physiological states of hunger and satiety. NeuroImage 44 (3), 1008–1021.
Hooks, B.M., Chen, C., 2020. Circuitry underlying experience-dependent plasticity in the mouse visual system. Neuron 106 (1), 21–36.
Hristovska, I., Verdonk, F., Comte, J.C., Tsai, E.S., Desestret, V., Honnorat, J., Chrétien, F., Pascual, O., 2020. Ketamine/xylazine and barbiturates modulate microglial morphology and motility differently in a mouse model. PLoS One 15 (8), e0236594.
Hsu, D.T., Kirouac, G.J., Zubieta, J.K., Bhatnagar, S., 2014. Contributions of the paraventricular thalamic nucleus in the regulation of stress, motivation, and mood. Front Behav. Neurosci. 8, 73.
Inada, K., Tsujimoto, K., Yoshida, M., Nishimori, K., Miyamichi, K., 2022. Oxytocin signaling in the posterior hypothalamus prevents hyperphagic obesity in mice. eLife 11, e75718.
Kasai, R., Nashi, K., Ohtani, K., Zhou, J., Tao, G.D., Tanaka, O., 1989. Sweet cucurbitane glycosides from fruits of Siraitia siamensis (chi-zi luo-han-guo), a Chinese folk medicine. Agricultural and Biological Chemistry, 53 (12), 3347–3349.
Kelley, A.E., Pratt, W., 2005. A proposed hypothalamic-thalamic-striatal axis for the integration of energy balance, arousal, and food reward. J. Comp. Neurol. 493, 72–85.
Knight, J.A., Chien, C.H., Wang, D., Panessiti, M., Ameroso, D., Greenberg, A., Feng, G., Kong, D., Rios, M., 2017. Alpha2delta-1 in SF1 + Neurons of the ventromedial hypothalamus is an essential regulator of glucose and lipid homeostasis. Cell Rep. 21 (10), 2737–2747.
Kujur, R., Singh, V., Ram, M., Yadava, H., Singh, K., Kumari, S., Roy, B., 2010. Antidiabetic Activity and Phytochemical Screening of Crude Extract of Stevia rebaudiana in Alloxan-induced Diabetiis Rats. Pharmacogn. Res. 2 (4), 258–263.

Labouèbe, G., Boutrel, B., Tarussio, D., Thorens, B., 2016. Glucose-responsive neurons of the paraventricular thalamus control sucrose-seeking behavior. Nat. Neurosci. 19 (8), 999–1002.

Lim, J.S., Snyder, M., Valente, A., Schwarz, J.M., Lustig, R.H., 2010. The role of fructose in the pathogenesis of NAFLD and the metabolic syndrome. Nat. Rev. Gastroenterol. Hepatol. 7 (5), 251–264.

Loney, G.C., Eckel, L.A., 2021. The pattern of fos-like immunoreactivity expressed within the nucleus of the solitary tract is associated with individual variation in the taste quality of a stimulus. Chem. Senses 46, bjab036.

Millan, E.Z., Ong, Z., McNally, G.P., 2017. Paraventricular thalamus: gateway to feeding, appetitive motivation, and drug addiction. Prog. Brain Res. 235, 113–137.

Mirochnik, R.M., Pezaris, J.S., 2019. Contemporary approaches to visual prostheses. Mil. Med Res 6 (1), 19.

Mishra, A., Ahmed, K., Froghi, S., Dasgupta, P., 2015. Systematic review of the relationship between artificial sweetener consumption and cancer in humans: analysis of 599,741 participants. Int. J. Clin. Pract. 69 (12), 1418–1426.

Mitchell, S., Shaw, D., 2015. The worldwide epidemic of female obesity. Best. Pr. Res Clin. Obstet. Gynaecol. 29 (3), 289–299.

Morton, G.J., 2007. Hypothalamic leptin regulation of energy homeostasis and glucose metabolism. J. Physiol. 583 (Pt 2), 437–443.

Mungarndee, S.S., Norgren, R., 2008. Expression of Fos during sham sucrose intake in rats with central gustatory lesions. Am. J. Physiol. Regul. Integr. Comp. Physiol. 295 (3), 751–763.

Otis, J., Zhu, M., Namboodiri, V., Cook, C., Kosyk, O., Matan, A., Ying, R., Hashikawa, Y., Hashikawa, K., Pisanty, I., Guo, J., Ung, R., Romaguera, J., Anton, E.S., Stuber, G., 2019. Paraventricular Thalamus projection neurons integrate cortical and hypothalamic signals for cue-reward processing. Neuron 103 (3), 423–431.

Park, H.W., Kim, M.J., Seo, S., Yoo, S., Hong, J.H., 2017. Relative sweetness and sweetness quality of Xylobiose. Food Sci. Biotechnol. 16 (3), 689–696.

Parsons, W., Greiner, E., Buczek, L., Migliaccio, J., Corbett, E., Madden, A.K., Petrovich, G.D., 2022. Sex differences in activation of extra-hypothalamic forebrain areas during hedonic eating. Brain Struct. Funct. 227 (8), 2857–2878.

Petrovich, G.D., 2018. Feeding behavior survival circuit: anticipation & competition. Curr. Opin. Behav. Sci. 24, 137–142.

Ren, S., Wang, Y., Yue, F., Cheng, X., Dang, R., Qiao, Q., Sun, X., Li, X., Jiang, Q., Yao, J., Qin, H., Wang, G., Liao, X., Gao, D., Xia, J., Zhang, J., Hu, B., Yan, J., Wang, Y., Xu, M., Han, Y., Tang, X., Chen, X., He, C., Hu, Z., 2018. The paraventricular thalamus is a critical thalamic area for wakefulness. Science 362 (6413), 429–434.

Rogers, P.J., Blundell, J.E., 1989. Separating the actions of sweetness and calories: effects of saccharin and carbohydrates on hunger and food intake in human subjects. Physiol. Behav. 45 (6), 1093–1099.

Smeets, P., Weijzen, P., Graaf, C., Viergever, M., 2011. Consumption of caloric and non-caloric versions of a soft drink differentially affects brain activation during tasting. NeuroImage 54 (2), 1367–1374.

Somayajulu, M., McClellan, S.A., Pitchaikannu, A., Bessert, D., Liu, L., Steinle, J., Hazlett, L.D., 2021. Effects of Glycyrrhizin Treatment on Diabetic Cornea. J. Ocul. Pharm. Ther. 37 (1), 12–23.

Sternson, S., Eiselt, A.K., 2017. Three pillars for the neural control of appetite. Annu. Rev. Physiol. 79.

Szatko, K.P., Korympidou, M.M., Ran, Y., Berens, P., Dalkara, D., Schubert, T., Euler, T., Franke, K., 2020. Neural circuits in the mouse retina support color vision in the upper visual field. Nat. Commun. 11, 3481.

Tellez, L., Han, W., Zhang, X., Ferreira, T., Perez, I., Lagnado, S., Pol, A., de Araujo, I., 2016. Separate circuitries encode the hedonic and nutritional values of sugar. Nat. Neurosci. 19 (3), 465–470.

Venditti, C., Veloso, K., Lee, H.Y., Poon, T., Mak, A., Darch, M., Juana, J., Fronda, D., Noori, D., Pateman, E., Jack, M., 2020. Determinants of sweetness preference: a scoping review of human studies. Nutrients 12 (3), 718.

Wang, S., Cui, K., Liu, J., Hu, J., Yan, K., Xiao, P., Lu, Y., Yang, X., Liang, X., 2022. Mogroside-rich extract from siraitia grosvenorii fruits ameliorates high-fat diet-induced obesity associated with the modulation of gut microbiota in mice. Front. Nutr. 9, 870394.

Wang, Q., Ding, S.L., Li, Y., Royall, J., Feng, D., Lesnar, P., Graddis, N., Naeemi, M., Facer, B., Ho, A., Dolbeare, T., Blanchard, B., Dee, N., Wakeman, W., Hirokawa, K.E., Szafer, A., Sunkin, S.M., Oh, S.W., Bernard, A., Phillips, J.W., Hawrylycz, M., Koch, C., Zeng, H., Harris, J.A., Ng, L., 2020. The Allen mouse brain common coordinate framework: a 3D reference atlas. Cell 181 (4), 936–953.

Yang, W., Guo, X., Tu, Z., Chen, X., Han, R., Liu, Y., Yan, S., Wang, Q., Wang, Z., Zhao, X., Zhang, Y., Xiong, X., Yang, H., Yin, P., Wan, H., Chen, X., Guo, J., Yan, X.X., Liao, L., Li, S., Li, X., 2022. PINK1 kinase dysfunction triggers neurodegeneration in the primate brain without impacting mitochondrial homeostasis. Protein Cell 13 (1), 26–46.

Yang, Y., Wei, Y., Guo, X., Qi, P., Zhu, H., Tang, W., 2019. Glycyrrhetic acid monoglucuronide: sweetness concentration-response and molecular mechanism as a naturally high-potency sweetener. Food Sci. Biotechnol. 28 (4), 1187–1193.

Yoshida, K., Kato, D., Sugio, S., Takeda, I., Wake, H., 2023. Activity-dependent oligodendrocyte calcium dynamics and their changes in Alzheimer's disease. Front. Cell. Neurosci. 17, 1154196.

Zhang, X., van den Pol, A.N., 2017. Rapid binge-like eating and body weight gain driven by zona incerta GABA neuron activation. Science 356 (6340), 853–859.

Zhu, Y., Nachtrab, G., Keyes, P., Allen, W., Luo, L., Chen, X., 2018. Dynamic salience processing in paraventricular thalamus gates associative learning. Science 362 (6413), 423–429.